JACS
JOURNAL OF THE AMERICAN CHEMICAL SOCIETY

Article

pubs.acs.org/JACS

Interdye Hole Transport Accelerates Recombination in Dye Sensitized Mesoporous Films

Davide Moia,[*,†] Anna Szumska,[†] Valérie Vaissier,[†,∥] Miquel Planells,[‡] Neil Robertson,[‡] Brian C. O'Regan,[§] Jenny Nelson,[†] and Piers R. F. Barnes[*,†]

[†]Blackett Laboratory, Imperial College London, Prince Consort Road, London SW7 2AZ, U.K.

[‡]EaStCHEM School of Chemistry, University of Edinburgh, King's Buildings, David Brewster Road, Edinburgh EH93FJ, U.K.

[§]Department of Chemistry, Imperial College London, London SW7 2AZ, U.K.

Supporting Information

ABSTRACT: Charge recombination between oxidized dyes attached to mesoporous TiO_2 and electrons in the TiO_2 was studied in inert electrolytes using transient absorption spectroscopy. Simultaneously, hole transport within the dye monolayers was monitored by transient absorption anisotropy. The rate of recombination decreased when hole transport was inhibited selectively, either by decreasing the dye surface coverage or by changing the electrolyte environment. From Monte Carlo simulations of electron and hole diffusion in a particle, modeled as a cubic structure, we identify the conditions under which hole lifetime depends on the hole diffusion coefficient for the case of normal (disorder free) diffusion. From simulations of transient absorption and transient absorption anisotropy, we find that the rate and the dispersive character of hole transport in the dye monolayer observed spectroscopically can be explained by incomplete coverage and disorder in the monolayer. We show that dispersive transport in the dye monolayer combined with inhomogeneity in the TiO_2 surface reactivity can contribute to the observed stretched electron−hole recombination dynamics and electron density dependence of hole lifetimes. Our experimental and computational analysis of lateral processes at interfaces can be applied to investigate and optimize charge transport and recombination in solar energy conversion devices using electrodes functionalized with molecular light absorbers and catalysts.

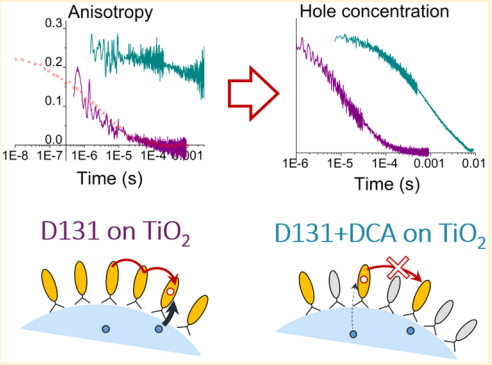

INTRODUCTION

The photogeneration and separation of charges at the interface of molecular systems represents the core energy conversion process of dye sensitized solar cells (DSSCs) and solar fuel cells.[1,2] The efficiency of these devices is reduced by fast recombination of electrons in the oxide and holes in the photo-oxidized dyes. Therefore, it would be beneficial to design systems with long charge lifetime (i.e., slow recombination).[3,4]

Investigation of the recombination process between electrons in titanium dioxide (TiO_2) and holes on surface anchored dyes is typically performed by characterizing films immersed in inert electrolytes. This guarantees that photogenerated holes are not transferred to the electrolyte and remain in the dye monolayer until they recombine with photogenerated electrons. Transient absorption spectroscopy (TAS) studies showed that electron hole recombination kinetics in dye sensitized TiO_2 nanocrystalline films in inert electrolytes depends on the electron density in the TiO_2 electrode.[1,5,6] However, the decay kinetics indicated that the recombination occurred with a wide distribution of time constants (a dispersive process) and could not be described by a simple second order model. These experimental observations were reproduced with simulations using a continuous time random walk (CTRW) model where the recombination process is limited by trapping-detrapping mediated transport of electrons in the TiO_2 reaching surface anchored oxidized dyes.[5,7] The model assumed an exponential density of trap states below the conduction band in TiO_2 described by the characteristic energy E_{ch}. The results from this model, used to describe the TAS decay of the photo-oxidized dye population, could also be analytically approximated by a stretched exponential function with stretching parameter $\alpha = k_BT/E_{ch}$ (where k_BT is the thermal energy).[6] Those studies identified that the half-life of the photogenerated holes, $t_{50\%}$, varied with the background electron density, n, according to $t_{50\%} \propto n^{-1/\alpha}$. Subsequent studies examined the influence of the chemical structure of the dye on the kinetics of the electron hole recombination reaction. The results presented evidence for systems showing longer lifetimes due to reaction limitations as opposed to electron transport limitation.[8−11] Thus, tuning surface properties[12,13] and modifying the dye chemical structure[9] have been emphasized as routes to minimize electron-dye recombination. On the other hand, other reports showed unchanged recombination dynamics upon change in dye chemical structure, suggesting that diffusion limited encounter

Received: May 13, 2016
Published: September 9, 2016

DOI: 10.1021/jacs.6b04956
J. Am. Chem. Soc. 2016, 138, 13197−13206

between electrons and holes represents the rate limiting process in some systems.[14,15] The studies described above focused on the transport of the electrons and on dye-surface interaction while assuming holes to be fixed on dye molecules after photogeneration.

However, hole transport between dyes anchored to the surface of mesoporous films has been demonstrated via electrochemical and spectroscopic techniques for sensitized films when the coverage of dyes on the surface exceeds a percolation threshold of about 50%.[16,17] This hole transport process has been applied to solar fuel systems,[18,19] batteries[20] and electrochromic devices.[21] In addition, we have recently shown that it plays a critical role in the photoconversion of solid state DSSCs, enabling efficient regeneration of the device despite incomplete coverage of the dyed mesostructure by the hole transporting material (HTM).[22] We have also demonstrated that it is possible to create working DSSCs that do not require a separate HTM since hole collection can be accomplished solely by the dye layer.[23] The possible influence of hole transport within dye monolayers on hole recombination with electrons in TiO_2 has been considered by Ogawa et al. Electron hole recombination for dye sensitized TiO_2 nanocrystalline films was measured using TAS for a series of organic dyes.[24] Decrease in recombination kinetics was observed when introducing nonconjugated side groups to the dyes' chemical structure. An increase in lifetime was also observed upon decreasing the dye surface coverage using the coadsorbent chenodeoxycholic acid (DCA). These results were attributed to the expected variation in the rate of hole transport in different dye monolayers. Other studies that consider the possibility for hole transport to play a role in the recombination dynamics have been reviewed in reference.[4]

In this work we measure the electron hole recombination kinetics using TAS and simultaneously measure hole diffusion in the dye monolayer using transient absorption anisotropy spectroscopy for dye sensitized TiO_2 nanocrystalline films immersed in inert electrolytes. We compare samples in which we control the rate of hole transport in the monolayer either by changing the dye surface coverage or the solvent surrounding the sample during the measurement. We also use Monte Carlo simulations to investigate the effect of different monolayer properties on the simulated transient anisotropy profile to aid the interpretations of the experimental results.

This study reveals that hole transfer between dyes influences charge recombination at heterogeneous interfaces and impacts the optimization of photoelectrochemical systems such as DSSCs and solar fuel devices. In addition, our joint experimental and computational approach represents a direct measure of charge transport properties of molecular semiconductors.

RESULTS AND DISCUSSION

Electron−Hole Recombination: The Effect of Dye Surface Coverage. Figure 1a and b show transient measurements of oxidized dye absorption following 450 nm wavelength laser pulse excitation of D131 sensitized TiO_2 electrodes with different dye surface coverage. The variation in transient optical density (ΔOD) reflects the population of oxidized dyes remaining, probed at 1000 nm wavelength, and hence the dynamics of hole recombination with electrons. The choice of wavelengths is discussed in Section 1 of the Supporting Information. Data are plotted for different values of the background electron concentration in TiO_2, n, controlled electrochemically (see Figure 1e) and measured via charge extraction. The measurements were performed on the sample immersed in an inert electrolyte (0.1 M *tert*-butyl ammonium perchlorate in acetonitrile) in a three electrode cell as discussed in the experimental section. The lifetime of the holes decreases substantially with increasing n in both cases of (a) high and (b) low D131 coverage, consistent with previous reports.[5] Figure 1c compares the half-life of the fully dyed D131 sensitized sample with samples where the D131 loading was decreased either by using a short dyeing time or by using the coadsorbent DCA to limit the uptake of the dye to the surface.[25] The case of partial dye desorption is also presented in Section 2 of the Supporting Information.

Figure 1c shows that hole lifetimes are consistently shorter for the sample with full coverage than for samples with decreased dye loading, even for concentrations of photogenerated electrons much lower than the total electron density ($n_{ph} < n/10$, see Experimental Section). This shows that, for D131 sensitized TiO_2 samples at equal electron densities, high dye loading correlates with faster electron hole recombination. The trend is observed up to electron concentration exceeding 10^{18} cm^{-3}, which is representative for DSSC devices operating at maximum power point under 1 sun illumination.[26] Also, the recorded recombination lifetimes in this region are in the order of microseconds. This is comparable to the kinetics of regeneration observed in DSSCs using redox couples which enable high open circuit voltage (V_{oc}) solar cells.[27] The recombination between holes on dyes and electrons in TiO_2 can therefore become important in solar cell devices under operating conditions.

We note that molecular orientations on the TiO_2 may be sensitive to the dye surface coverage conditions as well as to the presence of the inert coadsorbent. Although were not able to control this orientation experimentally, we expect that high surface packing in the dye monolayer may lead to an increase in the distance between photo generated holes from the TiO_2 surface. This would potentially result in slower interfacial reaction kinetics.[9] Since the high dye coverage case showed faster recombination than the lower coverage cases it is unlikely that molecular orientation plays a dominant role in the differences in recombination dynamics we observed.

In the next sections we investigate the hole transport properties of D131 sensitized samples and discuss how this process could contribute to recombination dynamics. In addition, we simulated the hole recombination kinetics for different electron densities using a model that includes the hole transport properties of the dye monolayer (see schematics in Figure 1e and 1f). The data are displayed in Figure 1d and will also be discussed in the next sections.

Hole Transport in the Dye Monolayer: Interpreting Transient Anisotropy Measurements. In Figure 2 we show measurements of transient absorption anisotropy under the same experimental conditions as the data shown in Figure 1 (0.1 M TBAP in acetonitrile). We also compare the experimental observations to simulations of the transient absorption anisotropy profile of holes diffusing in a dye monolayer arranged on the surface of a cubic particle (see Experimental Section). Transient absorption anisotropy spectroscopy involves monitoring time-resolved changes in absorption anisotropy of the sample following pulsed polarized photoexcitation. The measurement provides information on the transition dipole moment orientation of the photogenerated species, at a specific probe wavelength, with respect to the excitation polarization. In the particular case of a dye sensitized TiO_2 nanoparticle, pumping the sample with polarized light selectively excites a population of dyes whose transition dipole moments are aligned with the pump

DOI: 10.1021/jacs.6b04956
J. Am. Chem. Soc. 2016, 138, 13197−13206

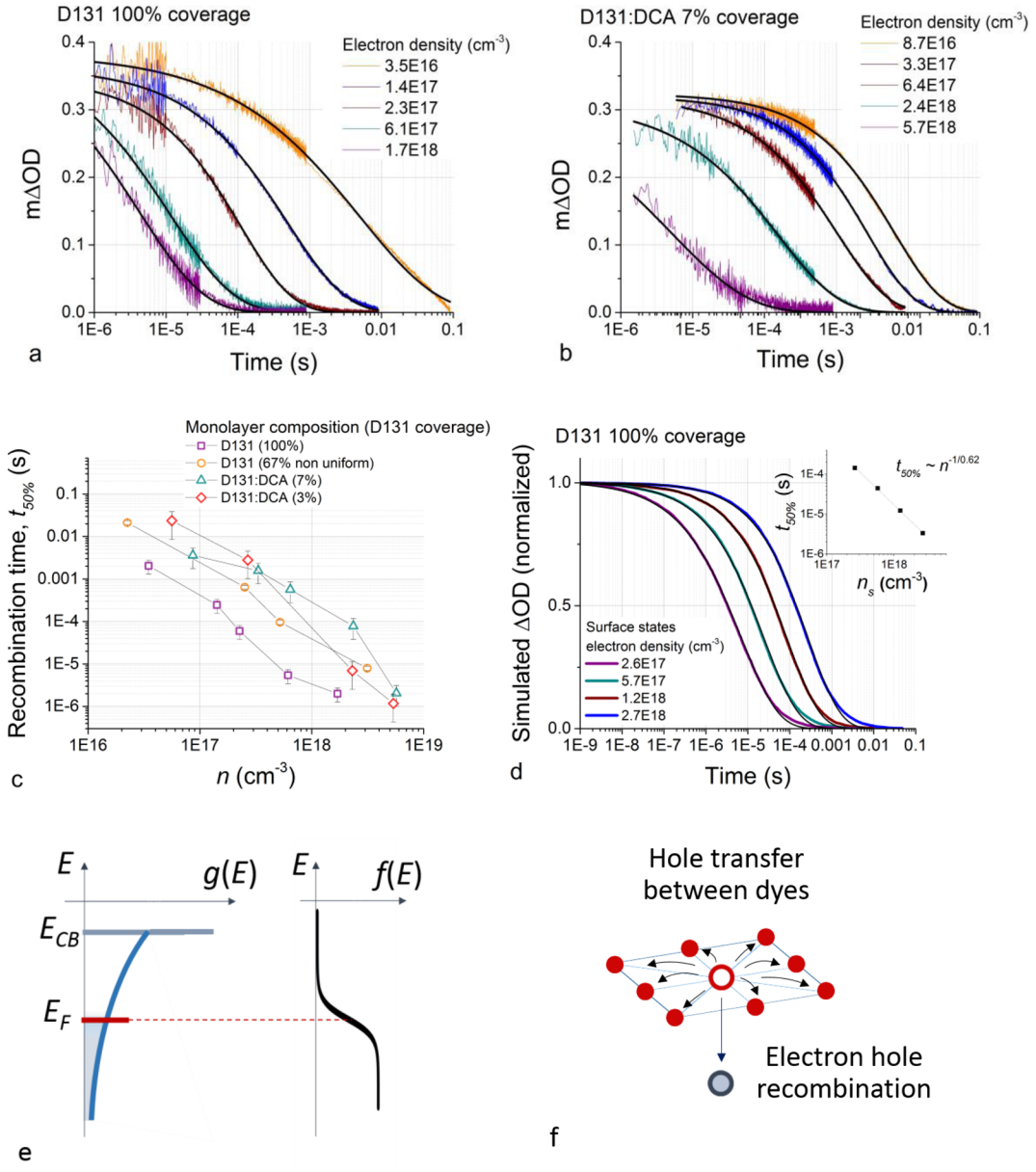

Figure 1. Transient absorption spectroscopy decays of (a) D131 and (b) D131:DCA sensitized TiO_2 nanocrystalline films in 0.1 M TBAP in acetonitrile. The measurements refer to different background electron concentration in the TiO_2, n, induced by the applied bias and calculated from charge extraction measurement (see Experimental Section). The samples were pumped with laser pulses at a wavelength of 450 nm and the oxidized dye population was probed at 1000 nm. (c) Half-life times as a function of electron concentration in the TiO_2 for D131 sensitized TiO_2 samples with full dye coverage (purple) and with decreased dye coverage. The low dye coverage was obtained by either short dyeing time, which we expect to yield non uniform dyeing, or D131:DCA cosensitization. The slope of $\log(t_{50\%})$ vs $\log(n)$ varies between $-(0.44)^{-1}$ and $-(0.62)^{-1}$ for the different samples. The coverage fractions refer to D131 and were determined via dye desorption, as described in Section 3 of the Supporting Information. Error bars were calculated based on the fractional variation in $t_{50\%}$ of TAS decays taken at open circuit before and after all the measurements. (d) Simulated hole recombination in D131 monolayer with electrons situated on the surface of $(20\ nm)^3$ TiO_2 particles. The black lines correspond to stretched exponentials fitted to the simulations. (e) Schematics of the density of states $g(E)$ in TiO_2 films and Fermi–Dirac distribution $f(E)$ as a function of electron energy. The position of the Fermi level E_F determines the background electron concentration n in the film. It is controlled with an applied bias in our experiments and it is an input parameter in our calculations. (f) Model of recombination used for the calculations displayed in Figure 1d. Hole transfer between dyes competes with recombination with electrons in the TiO_2.

polarization at the excitation wavelength. Electron injection in the TiO_2 leaves these dyes in the oxidized state which present different optical absorption features to the unoxidized molecule. Probing the changes in absorption polarization (transition dipole moment orientation) of the oxidized dyes at a convenient wavelength enables us to learn about the dynamics of photogenerated holes. In our case, the anisotropy probed at 1000 nm is expected to be dominated by the oxidized D131 component (see Section 1 of the Supporting Information). Previous studies have discussed the relation between the transient anisotropy profile of the oxidized dye absorption and the diffusion of the hole within the monolayer.[18,22] They concluded that decay in anisotropy can be interpreted in terms of holes being transferred between dyes with different orientation.

DOI: 10.1021/jacs.6b04956
J. Am. Chem. Soc. 2016, 138, 13197–13206

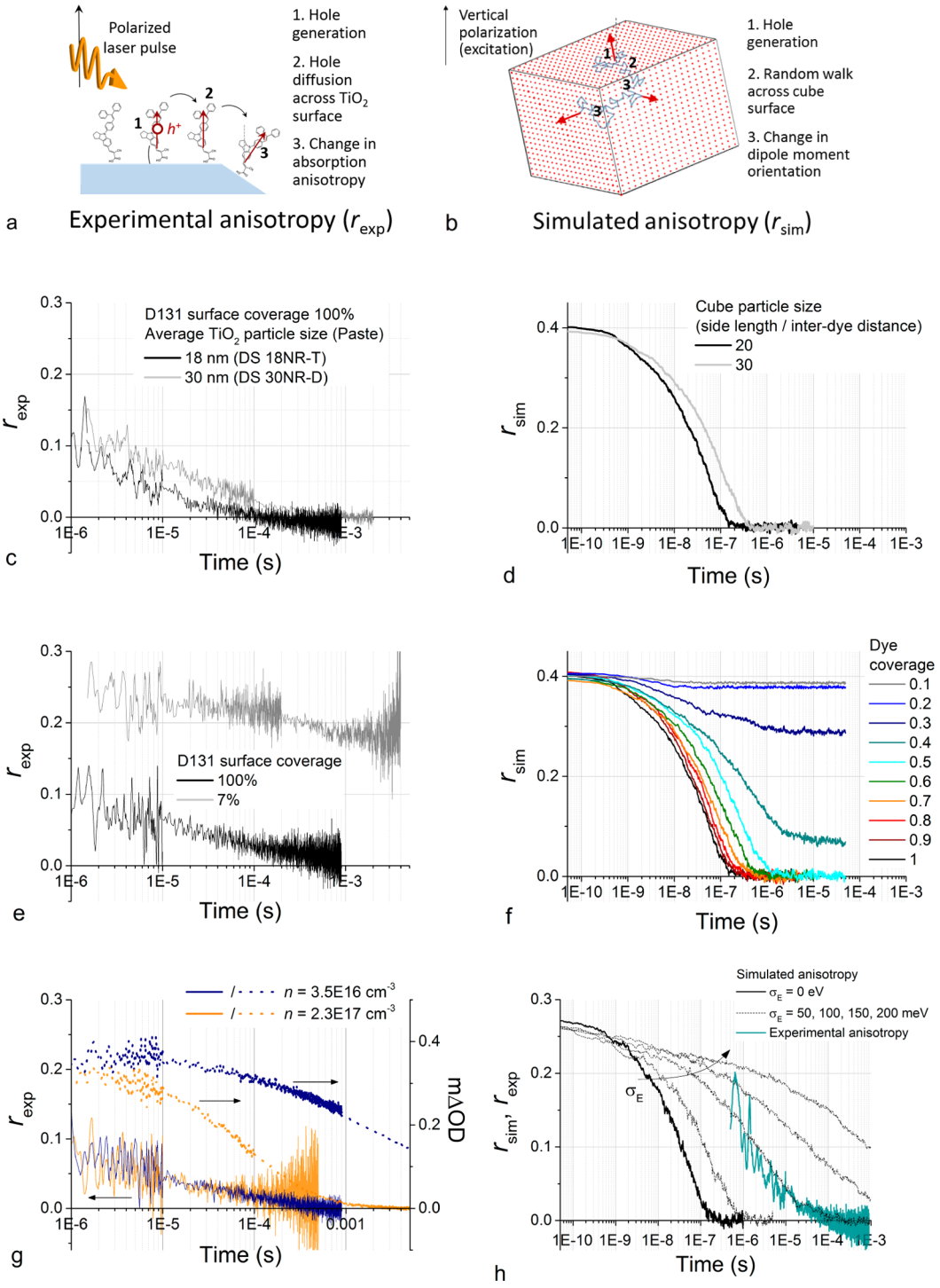

Figure 2. Schematics of (a) experimental and (b) simulated transient absorption anisotropy spectroscopy on D131 sensitized TiO_2 nanocrystalline films in 0.1 M TBAP in acetonitrile. (c) Experimental and (d) simulated anisotropy decay for fully dyed D131 TiO_2 with different TiO_2 average particle size (diameter). (e) Anisotropy decay measured for films with full (100%) D131 coverage and with partial (7%) D131 coverage obtained by cosensitizing with D131:DCA. The TAS decay for these samples is shown in Figure 1a and b. (f) Simulated coverage dependence of transient absorption anisotropy. (g) Anisotropy (left axis) and TAS (right axis) decays measured for a fully dyed D131 TiO_2 film with different electrochemically induced electron concentrations in the TiO_2 film (see legend). (h) Comparison between experimental anisotropy and simulated anisotropy decays for the complete dye coverage case including the effect of energetic disorder in the simulation (σ_E is the standard deviation of the Gaussian distribution used to assign site energies). The simulated transient absorption anisotropy decays refer to dyes arranged on the surface of a cube where each facet has 20 × 20 available sites. Values of electronic coupling J = 18 meV and reorganization energy λ = 1.062 eV were used in the model. For simulations displayed in (d) and (f) we considered the case of transition dipole moments oriented perpendicular to the cube surface. Simulations shown in (h) considers an angle of 152.6° between the unoxidized dye's transition dipole moment (oriented perpendicular to the surface) and oxidized dye's transition dipole moment, based on our TD-DFT analysis (see Section 1 and 4 in the Supporting Information).

DOI: 10.1021/jacs.6b04956
J. Am. Chem. Soc. 2016, 138, 13197−13206

Changes in such orientation occur when the hole is transferred to dyes that are anchored to sites of a particle with different surface orientations, suggesting that experimental anisotropy decays could be directly interpreted in terms of distance traveled by holes. For example, in the case of hole diffusion on a spherical surface where the dyes' transition dipole moments are oriented perpendicular to the surface, anisotropy is expected to decay monoexponentially.[18] On the other hand, neighboring dyes can present different orientation due to different molecular configurations with respect to the surface, implying that evaluating the rate of diffusion from transient anisotropy decays requires detailed knowledge of the system (see full discussion in Section 4 of the Supporting Information). In Figure 2c we compare the transient anisotropy decay for mesoporous films made with different TiO_2 particle sizes (18 versus 30 nm diameter) both with full coverage of D131. This comparison shows that hole transport in dye monolayers sensitizing larger size particles results in slower anisotropy decay dynamics. Assuming that this correlation is causal, then this suggests that, for D131 on TiO_2, photogenerated holes must cover distances in the order of the particle size to obtain complete decay of this quantity. The numerical model used for Figure 2d and 2f considers dyes adsorbed on a cubic particle where dyes on the same facet show identical transition dipole moments orientation. In this case, changes in anisotropy only occur when the hole diffuses across a facet edge. On the basis of the above observation about particle size dependence, the model should be at least in part representative of the real system. Figure 2d compares the simulated decay in anisotropy for different size of the cubic particle, reproducing qualitatively the difference in the profiles obtained for the experimental results. The factors influencing the profile (amplitude, dispersion and time scale of the decay) of the simulated anisotropy will be considered further below.

Figure 2e shows that, for a fully dyed sample, the transient anisotropy signal decays within few hundreds of microseconds. On the other hand, when the D131 coverage is low, the transient anisotropy signal at the earliest time-resolved is about 0.25 and shows incomplete decay up to millisecond time scale. The values of anisotropy recorded are lower than 0.4 which is the theoretical maximum value for isotropic samples. 0.25 is likely to be the highest anisotropy achievable for this dye, due to the relative orientation of the transition dipole moments that are involved in the excitation of the dyes and probing of the oxidized dyes (more details can be found in Section 1 and 4 of the Supporting Information). Slow decay in anisotropy is observed also for the other low coverage samples (see Section 2 of the Supporting Information). These results are in qualitative agreement with Figure 2f where the simulated anisotropy profiles follow different dynamics depending on the surface coverage. In particular for surface coverage <50% incomplete decay is observed. This is consistent with confinement of some holes on isolated islands of dyes on particular surface orientations of the particles.

Figure 2g shows measurements of transient absorption anisotropy and the respective TAS decay on a D131 sample while applying two different electrochemical potentials to the TiO_2 electrode, which result in different background electron concentrations measured by charge extraction. When increasing the electron concentration by a factor of 6.5, the anisotropy decay shows no noticeable difference even though the lifetime of the holes is significantly decreased (by a factor of 33). This implies that electrons in the TiO_2 do not significantly influence the rate of hole transport in the dye monolayer. We therefore assume that, for all the traces displayed in Figure 1a, hole diffusion kinetics in the dye monolayer are the same.

The stretching shown for simulated transient absorption anisotropy of full coverage samples (Figure 2d,f) is much less pronounced than the one observed experimentally (see Figure 2c,e,g). From Figure 2f, we note that dispersion increases slightly when less than 100% coverage is considered and becomes important when approaching 40−50% coverage. Interconnection between sites occupied by dyes becomes poor and hinders the diffusion of the charges across the particle's surface. The transition between the conditions of well and poorly interconnected network of dyes can be defined as the percolation threshold. We conclude that local incomplete coverage may contribute to the observed dynamics. In addition, other sources of dispersion in time constant are likely to play a role in determining the stretched profile of the transient absorption anisotropy. In particular, we identify the following main factors: disorder in dye site energies (Figure 2h) and in relative spacing or interaction between neighboring dyes; distribution in the relative orientation of the dyes' transition dipole moments; distribution in size and shape of the nanoparticles used experimentally (see full discussion of these factors in Section 4 of the Supporting Information). We also show that energetic disorder in the monolayer results in an overestimate of the "apparent" reorganization energy for intermolecular charge transfer (see Figure S7). This observation is expected for transport in disordered systems and represents a potential explanation for the discrepancy between measured and calculated values of reorganization energy in our earlier report.[28]

On the basis of these results and our previous investigations, our current interpretation of the hole hopping process in the (D131) dye monolayer is as follows: hole transport between dyes anchored to the surface of TiO_2 particles occurs in samples with dye coverage exceeding the percolation threshold and does not significantly depend on the electron density in the TiO_2 scaffold. The stretched anisotropy decays (Figure 2) indicate pronounced dispersion in the transport of holes in the dye monolayer across different surface orientations of the nanoparticle. This can be explained by considering local incomplete coverage and/or energetic disorder between different sites. The latter factor increases the apparent activation energy for transport. This can be extracted from temperature dependent electrochemical measurements. Dye fluctuation may be responsible for the relatively high hole diffusion coefficient and electronic coupling that we extract from cyclic voltammetry.[29] Finally, below the percolation threshold, diffusion of the holes on the surface is hindered due to the limited number of connected paths formed by the dyes. This interpretation enables us to simulate electron hole recombination accounting for hole diffusion properties of the dye monolayer as we discuss in the next sections.

Electron−Hole Recombination and Hole Transport between Dyes. We now consider the mechanism by which lateral hole transport described in the previous section and Figure 2 could influence the trend in recombination displayed in Figure 1.

Our interpretation of the transient anisotropy measurements shown in this study suggests that the trend of increasing hole lifetime with decreasing dye coverage seen in Figure 1c can be explained in terms of slower hole transport, i.e., inhibiting hole transport by reducing the dye surface coverage correlates with decreased rate of electron−hole recombination. This implies that, in addition to electron transport in the TiO_2 and interfacial electron−hole reaction, the dynamics of hole transport could be

DOI: 10.1021/jacs.6b04956
J. Am. Chem. Soc. 2016, 138, 13197−13206

contributing to the observed kinetics of the decay in photogenerated hole population measured with TAS.

The relation between charge transport properties and recombination kinetics in a system depends on the dimensionality of the phases populated by the charges and on the type of "interface" between such phases where recombination occurs. For example, when electrons and holes share the same phase, the recombination rate constant is expected to depend on the sum of the charge mobilities (Langevin recombination). Conversely, when electrons and holes are transported in two separate phases and need to reach an interface in order for recombination to occur, then the rate of collision of electrons with holes is limited by the slowest charge carrier's mobility.[30] Recombination between electrons in nanoparticles and holes in the dye monolayer adsorbed to the nanoparticle represents another type of system where one of the charge carriers (holes) is permanently exposed to the recombination interface, while the other (electrons) is not.

Figure 3 shows the simulated dependence of hole lifetime on the electron and hole diffusion coefficients for the case of a cubic

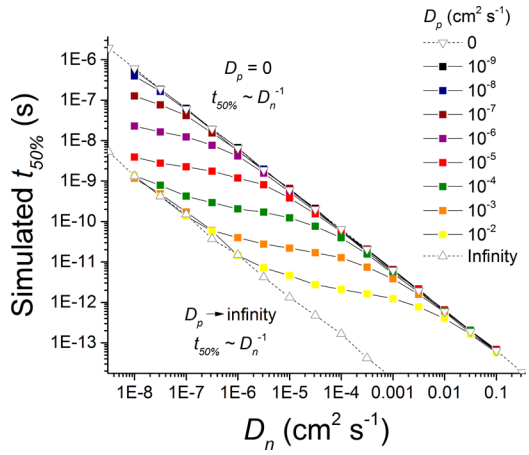

Figure 3. Simulated hole lifetime in a (disorder free) dye sensitized cubic nanoparticle as a function of the electron and the hole diffusion coefficients.

particle populated with one hole (diffusing on the surface of the cube) and one electron (diffusing within the volume of the cube). For this simulation we considered the case of recombination being limited by collision of the two charges, hence charges recombine when they approach each other within a certain distance (in this case, $\sqrt{3}$ times the lattice parameter).

We can identify three regimes in the recombination kinetics of this system. First, when hole transport in the monolayer is slower than electron transport in the bulk of the particle, recombination is limited by electron diffusion to the interface and to the site where the hole is localized. As a results, $t_{50\%}$ is proportional to D_n^{-1}, as it is also expected for the case of immobile holes ($D_p = 0$). When holes move significantly faster in the dye monolayer than electrons within the particle, the recombination time approaches the time that it takes for the electron to diffuse to any site at the interface (since the time taken by the hole to explore the whole particle surface is comparatively negligible). This regime also shows a $t_{50\%} \sim D_n^{-1}$ behavior. In the intermediate regime the hole diffusion coefficient is equal or greater by only few orders of magnitude than the electron diffusion coefficient and the recombination lifetime is dependent on both these quantities.

However, the condition $D_p > D_n$ is not expected for the case of data presented in Figure 1a, b and c, at least for the high electron density conditions, therefore this model cannot quantitatively explain our experimental observation. We note that a more complete model is needed to account for the disorder in the TiO_2 and in the dye monolayer, which is expected to influence these regimes of electron hole recombination. We address this factor in the next section.

The Effect of Disorder on Recombination. The effect of energetic disorder and dispersive electron transport in mesoporous TiO_2 on the stretched electron–hole recombination kinetics and electron density dependence of holes lifetime has been extensively investigated (see introduction). Below, we discuss the possibility that dispersive transport in the *dye monolayer* could also contribute to experimental observations of stretched recombination kinetics.

In order to explore this hypothesis, we consider a simplified model for the recombination process where electron transport within the TiO_2 particle is not a rate limiting factor. We focus instead on the effect of hole transport and disorder in the dye monolayer on the simulated recombination kinetics. We find that energetic disorder in the dye monolayer *combined with* inhomogeneity in the TiO_2 surface reactivity can introduce significant dispersion in the hole population decay as well as electron density dependence of the hole lifetime which deviates from a first order reaction ($t_{50\%} \sim n^{-1}$). We note that inhomogeneity in surface reactivity of anatase TiO_2 nanoparticles is expected, and has been shown previously.[31] In our model we consider energetic disorder for the TiO_2 surface states as a source of such inhomogeneity. In Figure 1d we show the simulated results of electron hole recombination given the model described in the Experimental Section and in detail in Section 5 of the Supporting Information. These simulations refer to the same hole transport parameters used for the data in Figure 2h (for σ_E = 100 meV) while the energetic disorder in the TiO_2 surface is obtained by assigning electronic energy levels drawn from an exponential density of states for each of the cubic particle's surface sites. In the model, the energetic disorder for the surface sites in the TiO_2 affects the hole recombination rate to each site, which is calculated to be proportional to the TiO_2 electronic site occupancy, given the Fermi level position used in the simulation. The surface site energies and the energetic disorder in the dye monolayer used in our model are uncorrelated. Figure 1d (along with Figure S9) shows that the model produces results: with a similar time scale and dispersion to the data displayed in Figure 1a for the transient absorption measurement of electron–hole recombination; and with a charge density dependence of the half-life which reproduces the experimental observation. In particular, Figure S9 and table S1 of the Supporting Information illustrate that both disorder in the monolayer and in the TiO_2 surface reactivity have to be present in order to observe these effects. In the model we have focused on the case of energetic disorder for both hole transport and the TiO_2 surface, however we would potentially expect an analogous trend to result from other sources of disorder.

The only free parameters in the model are the charge transfer rate between electronic states in the TiO_2 and oxidized dyes and the position of the conduction band edge. We discuss the sensitivity of the model to these quantities in Section 5 of the Supporting Information. The model reproduces the pronounced deceleration in recombination kinetics when the dye surface coverage is reduced below the percolation threshold observed experimentally.

DOI: 10.1021/jacs.6b04956
J. Am. Chem. Soc. 2016, 138, 13197–13206

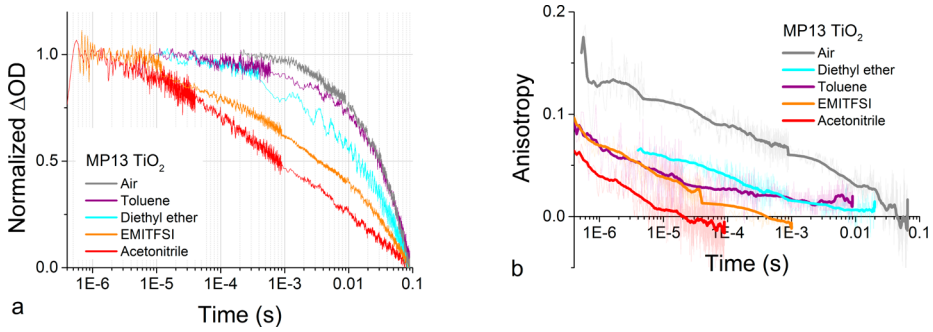

Figure 4. (a) Transient absorption and (b) transient absorption anisotropy spectroscopy on MP13 sensitized TiO_2 films on glass immersed in different environments. The films were pumped with pulsed laser excitation at 430 nm while the oxidized dye signal was probed at 770 nm. The solid lines in (b) are obtained by calculating a moving average of the raw data (also displayed in background).

Table 1. Values of Viscosity, Static Dielectric Constant (ε_r) and Refractive Index[a]

solvent	viscosity (mPa s) at 25 °C	ε_r at 20 °C	refractive index (temperature)	ε_{eff}^{-1}
acetonitrile	0.37	36.6	1.3442 (30 °C)	0.526
diethyl ether	0.224	4.27	1.3526 (20 °C)	0.312
toluene	0.56	2.38	1.4961 (20 °C)	0.0266
EMITFSI	88	<10	1.4305 (20 °C)	$0.39 < \varepsilon_{eff}^{-1} < 0.49$
air	0.019	1	1	0

[a]Taken from reference[32,16] for EMITFSI and from reference[33] for other solvents. The value of the Pekar factor (ε_{eff}^{-1}) is calculated as $\varepsilon_{eff}^{-1} = \varepsilon_{opt}^{-1} - \varepsilon_r^{-1}$, where ε_{opt} is the square of the refractive index.

Hole Transport between Dyes and Electron–Hole Recombination: The Effect of the Solvent. To further investigate the correlation between hole transport in the dye monolayer and electron hole recombination, we measured samples consisting of nominally identical MP13 sensitized TiO_2 films (with 100% dye surface coverage) exposed to different solvent environments. MP13 was chosen as it shows lower degree of desorption when immersed in the solvents investigated and better photostability than D131. Figure 4 shows the TAS and the transient absorption anisotropy decays for holes in MP13 sensitized TiO_2 films immersed in 4 different solvents and air. Both the dynamics of electron hole recombination and of hole diffusion undergo a remarkable change when changing the environment. Comparison of the recombination and the transient anisotropy decays between measurements shows that fast anisotropy decay, hence fast hole transport in the dye monolayer, correlates with fast electron hole recombination. One possible explanation for this set of data is therefore that the ability of holes to move on the surface of the particle catalyzes the recombination with electrons in the TiO_2. This would be consistent with our interpretation of the results displayed in Figure 1c.

We note that the extent to which the transient anisotropy varies when holes hop between neighboring molecules depends on the relative configuration of the molecules (see Section 4 of the Supporting Information). For this reason, a direct and quantitative comparison of the anisotropy decays in Figure 4b may not be reliable at this level of description. For the scope of this paper, the comparison of the decay time scales for the different solvent systems is still informative if we simply view the different solvents as a means to empirically change the hole transport rate.

In Table 1, some of the properties of the solvents used are displayed. No clear trend is found between the kinetics of hole transport and the viscosity of the solvent, suggesting that this factor does not play a primary role in the determination of charge diffusion between dyes. We observe that faster dynamics for the transient anisotropy decay correlates with higher Pekar factor ε_{eff}^{-1}, defined as $\varepsilon_{eff}^{-1} = \varepsilon_{opt}^{-1} - \varepsilon_r^{-1}$ (where ε_{opt} and ε_r are the optical and static dielectric constants of the solvent). This is in contrast with what would be expected for interdye hole transfer in a solvent environment within the nonadiabatic Marcus theory. When the environment is treated as a continuous medium, the outer sphere reorganization energy for charge transfer is proportional to the Pekar factor, implying that for environments showing high Pekar factors a slower transfer rate would be expected.[18,23] A similar trend was observed for estimates of the hole diffusion coefficient in dye sensitized oxide films from electrochemical measurements where ions are present in electrolytes. The diffusion coefficient was found to increase using solvents with increasing polarity.[16] The results were explained in terms of faster charge compensation by the ions in polar solvents upon interdye hole transfer where ion pairing is less pronounced than in nonpolar solvents. In our experiments, the same trend is found in absence of electrolyte ions, ruling out the role of ionic charge compensation as a limiting step for charge transport for our system. This observation questions the validity of predicting charge transfer rates in these weakly coupled systems on the basis of the expected outer sphere reorganization energies according to nonadiabatic Marcus' theory. Considering the surrounding solvent as a dielectric continuum may represent one key limitation. We also note that the reorganization energy is not the only parameter which is affected by the surrounding medium. Different solvents may influence the configuration of the molecules on the surface, thus influencing the transport rate. In particular, the coupling between dyes is highly sensitive to the packing of the monolayer and eventual change in order. One possibility is that the use of polar solvent results in more favorable configurations of the dyes for charge transport. The change in the electrostatic environment could also vary the energetic disorder in the monolayer.

DOI: 10.1021/jacs.6b04956
J. Am. Chem. Soc. 2016, 138, 13197–13206

The different solvents used here are expected to result in different outer sphere reorganization energies of charge transfer between dyes, but also different outer sphere reorganization energies for the electron transfer from TiO_2 to oxidized dyes. Assuming that the latter process occurs in the Marcus inverted region, higher reorganization energy would result in faster rates of charge transfer.[34,35] The results shown in Figure 4a could therefore also be interpreted on the basis of increasing Pekar factor resulting in faster recombination reaction upon electron hole encounter. This interpretation assumes that the electron transfer reaction between TiO_2 and the dyes is the limiting factor to the rate of recombination, as opposed to the electron transport to the dye-TiO_2 interface. On a related note, the solvent surrounding the sensitized film is expected to vary the oxidation potential of the dye. This influences the difference in free energy describing the charge recombination reaction and ultimately its rate. We note that a complete model describing recombination in dye-TiO_2 systems as a Marcus' inverted region reaction is still missing.[36,37] In addition to these factors, the use of different solvents may vary the TiO_2 density of states and mobility of electrons in the film. This effect could also contribute to the observed trend.

In a previous report by Bonhôte et al., hole transport through the dye monolayer to the FTO contact in DSSCs was considered as a possible route for faster electron−hole recombination.[11] In our study correlation between hole transport and hole lifetime is observed for samples fabricated on glass substrates or including a TiO_2 compact layer covering the FTO contact indicating that hole transfer to electrons in the FTO does not contribute to the observed trend in recombination kinetics.

CONCLUSIONS

We have shown experimental evidence that hole transport in high coverage dye layers anchored to the TiO_2 nanoparticles increases the rate of recombination of photogenerated holes with electrons in the oxide. We demonstrated that reducing the rate of recombination (and the rate of hole transport) can be achieved by either reducing the dye surface coverage or by using solvents showing low Pekar factor. Using Monte Carlo simulations we identified three kinetic regimes of recombination for a cubic particle depending on the relative magnitude of electron and hole diffusion coefficients. The measurements of hole diffusion in the dye monolayer via transient anisotropy spectroscopy suggests that this process is highly dispersive. We simulated the transient anisotropy signal and electron hole recombination using model inputs based on our previous electrochemical and computational investigations of hole hopping between dyes. The observed dispersive character of hole transport can be explained by considering the effect of disorder and incomplete coverage in the monolayer. We also showed that dispersive hole transport, combined with spatial inhomogeneity in interfacial recombination with electrons in the TiO_2, contributes to the dispersion in the hole population decay observed with transient absorption measurements and to the electron density dependence of hole lifetime. The significant increase in the lifetime of photogenerated charges that we induced by reducing dye coverage or using solvents with low Pekar factor has important implications for both DSSCs architectures where electron recombination with oxidized dyes limits their V_{oc}, and solar fuel devices where surface adsorbates catalyze slow chemical reactions. Together with our previous reports, this study emphasizes the importance of characterizing recombination of photogenerated charges in molecular sensitized mesoporous films in conjunction with the investigation of the charge transport properties of the dye layer. These insights suggest approaches to control intermolecular lateral processes, as opposed to other interfacial properties, as a route to improve device performance. We have also shown that studying lateral transport in dye monolayers is a useful strategy to test the validity of electron transfer theories adopted to model charge transfer events in these systems. Our data show that the solvent dependence of hole transport between dyes cannot be explained on the basis of the expected variation in reorganization energy of charge transfer and the use of nonadiabatic Marcus theory.

EXPERIMENTAL SECTION

Sample preparation and spectroscopy measurements were carried out using the setup and methods described in the literature.[28,38,22] These can be found in Section 3 of the Supporting Information.

The transient anisotropy $r_{exp}(t)$ was calculated from the measurements of transient optical density for vertical and horizontal polarization of the probe beam ($\Delta OD_V(t)$ and $\Delta OD_H(t)$, respectively), following a vertically polarized optical pump pulse, as

$$r_{exp}(t) = \frac{\Delta OD_V(t) - \Delta OD_H(t)}{\Delta OD_V(t) + 2\Delta OD_H(t)} \quad (1)$$

For all the anisotropy measurements shown in this study, ΔOD_V has been calculated as the average of a measurement taken before and after the measurement of ΔOD_H, to approximately compensate for any degradation of the film. This was significant for some of the samples as we show in Section 6 of the Supporting Information. TAS and transient anisotropy measurements were performed on D131 (purchased from Mitsubishi paper mills limited) and MP13 (chemical synthesis is illustrated in Section 7 of the Supporting Information) sensitized TiO_2. Samples with incomplete D131 coverage were fabricated by either adopting short dyeing time or by using the inert coadsorbent chenodeoxycholic acid (DCA, purchased from Sigma-Aldrich). The chemical structure of the dyes and the DCA molecule are shown in Figure 5.

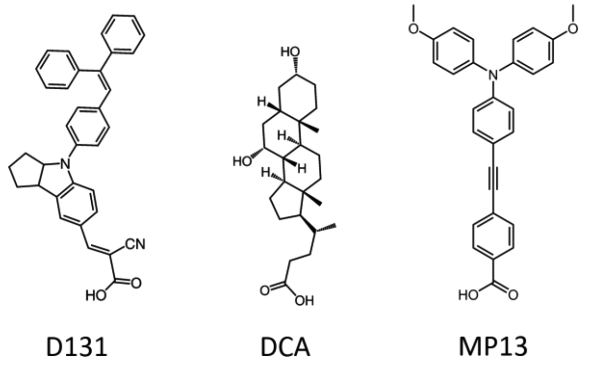

Figure 5. Chemical structure of the D131 and MP13 dyes and of the inert coadsorbent chenodeoxycholic acid (DCA).

The TiO_2 nanoparticle pastes were purchased from Dyesol. The paste 18NR-T (18 nm average particle size) was used for all experiments apart from results displayed in Figure 2c where a sample fabricated using the paste 30NR-D (30 nm average particle size) is also considered.

The measurements of D131 sensitized samples were carried out at controlled electrical potentials in an electrochemical cell. The cell was sealed and the electrolyte was flushed with argon for 20 min before the beginning of the measurements. The flow of argon was left blowing on top of the solution during all measurements to guarantee oxygen free environment. This was done to prevent electrochemically induced or photogenerated electrons reacting with oxygen. The dyed TiO_2 sample was used as working electrode in a three electrode configuration, a silver wire and a platinum electrode were used as quasi reference and counter

DOI: 10.1021/jacs.6b04956
J. Am. Chem. Soc. 2016, 138, 13197−13206

electrodes, respectively. Spectroscopy measurements were carried out while applying different potential values at the working electrode. For each trace, starting from a potential of 0.2 V vs silver wire quasi reference electrode, the working electrode was switched to the desired potential (between 0 V and −0.5 V vs silver wire). The TAS measurement was performed under these conditions. The working electrode was then switched back to 0.2 V at the end of the TAS measurement. The electron density in the film (n) was calculated by integrating the measured current density from the last of the three steps. The measured signal is expected to be related to the electron density in the TiO_2 during the TAS measurement. A nonzero current was recorded even after long time, suggesting a faradaic component due to electrons exchanged with the electrolyte. The reported values of charge density refer to the integrated current over a constant period of 60 s. The current density value at 60 s was subtracted to compensate for the baseline faradaic current (see Section 2 of the Supporting Information). The charge density, n, was not corrected for film porosity. The potential of the silver wire was measured before and after each measurement. Fluctuations of its potential with average of 60 mV and ranging between 20 mV and 250 mV were recorded before and after an experiment. By analyzing the recombination dynamics as a function of electron density we avoid the possible issue of potential drift for different measurements and between samples. When relating the spectroscopic data to the charge density measurement, we assume that the background concentration of electrons is homogeneous within the TiO_2 film, while we expect the profile of photogenerated electrons n_{ph} to vary through the depth of the film. The peak concentration of photoexcited dyes in D131 sensitized TiO_2 films by each laser pulse at the fluence used in the experiment is about 8×10^{16} cm^{-3} for the 100% coverage sample and 2.4×10^{15} cm^{-3} for the lowest dye coverage sample. Considering porosity of the film of 0.6 and approximating the TiO_2 particles as spheres of 10 nm radius, these values correspond to about 0.8 and 0.025 photoexcited dyes per particle.

The same spectroscopic characterization measurements (TAS and anisotropy) were made on MP13 sensitized TiO_2 films fabricated on glass without controlling the electrochemical potential of the samples.

Stretched exponential functions (eq 2) were fitted to the decays.

$$\Delta OD_{fit}(t) = A\exp\left[-\left(\frac{t}{\tau}\right)^{\alpha}\right] \quad (2)$$

In eq 2, α is the stretching parameter and τ the time constant. Half-life times were calculated from the fits using eq 3.

$$t_{50\%} = \tau(\ln 2)^{1/\alpha} \quad (3)$$

For most MP13 samples a background concentration of holes was present during the TAS measurements. This implies that half-life times for the incomplete decays would be longer than the ones that would be extracted from the data presented. Since the accumulation of background charges speeds up otherwise very slow recombination dynamics, this does not vary the relative trend of the kinetics observed between different measurements.

Monte Carlo Simulations. simulations of transient absorption anisotropy were carried out considering a square lattice of sites (dye monolayer) on the surface of a cube (TiO_2 nanocrystal). The data presented in the results section correspond to simulations of hole transfer between D131 dyes on the surface of a cubic TiO_2 particle of 20^3 nm^3 in size. Interdye distance was approximated to 1 nm. In the model, one hole at a time is considered per simulated experiment. The hole can be exchanged only between sites occupied by dyes and between up to 8 nearest neighbors. The kinetics of hole transfer between available sites are calculated using adaptive waiting times, which is expressed as a function of the nonadiabatic Marcus' charge transfer rate (see Section 3 in the Supporting Information). The reorganization energy of charge transfer was calculated as reported in a previous study, and the case of 0.1 M ions in acetonitrile was considered to match the experimental conditions.[39] In the disorder free case, the electronic coupling was taken from the experimental estimate reported in reference[28] (see Section 3 of the Supporting Information for more details). To introduce configurational disorder in the dye monolayer, a Gaussian distribution of calculated electronic couplings between sites was used (the distribution was for log J). Similarly, a Gaussian distribution of calculated site energy differences was implemented to simulate energetic disorder in the monolayer.

In order to simulate the transient absorption anisotropy profile expected for photogenerated holes diffusing in the dye monolayer, assumptions on the orientation of the transition dipole moments of the dye have to be taken. Calculations presented in Figure 2d, 2f consider the simplified case where the neutral state and oxidized state transition dipole moments are parallel. Under these conditions, our simulated profiles show initial values of 0.4, which is the maximum value expected for anisotropy measurement in isotropic systems. The transient anisotropy profile describes the change in orientation of the transition dipole moment of the oxidized dyes population in time. Therefore, the distribution of transition dipole moment orientations for the oxidized dyes on the surface of the particle influences the dynamics of the transient anisotropy decay. By considering all dipoles to be perpendicular to the surface of the particle, changes in anisotropy for each random walk experiment are recorded only upon hole exchange between different facets. Figure 2h refer to calculations where the relative orientation of the unoxidized and oxidized D131 dyes are take into account (see TD-DFT calcualtions in Section 1 of the Supporting Information). For this case, the unoxidized transition dipole moment is still set to be perpendicular to the cube surface, while the oxidized D131 dipoles are oriented at 152.6° from the normal. A rotation about the normal by a random angle is also applied to these dipoles for all dyes at the beginning of all random walk experiments. We discuss these and other aspects of accounting for transition dipole moment and dye backbone orientation in in Section 4 of the Supporting Information.

The facet where the hole was placed at $t = 0$ for each experiment was picked on the basis of a probability proportional to $\cos^2\vartheta$, where ϑ is the angle between the polarization axis of the excitation and the normal vector to the facet's surface. When running the random walk experiment, the square projection of the dipole moment of the oxidized dye in the direction parallel and in one of the directions perpendicular to the polarization axis were recorded. These quantities were averaged over time for all experiments and finally used to calculate the simulated anisotropy decay using eq 1. The random walk was ended after a certain time. This was the same for all experiments in a simulation. Each experiment takes into account a different orientation of the cubic particle with reference to the polarization axis of the excitation which was instead kept constant. Each simulated anisotropy profile presented here represents the average of 10^4 experiments.

Simulation of electron hole recombination dynamics shown in Figure 1d and in Section 5 of the Supporting Information were carried out using a model that considers one surface electronic state for the TiO_2 associated with each dye site. The energy of each state is drawn from an exponential distribution based on experimental observation (see charge extraction measurements in Section 2 of the Supporting Information). All states share the same quasi Fermi level; i.e., we consider electron transport in the TiO_2 to be significantly faster than hole transport in the dye monolayer and electron−hole recombination, such that all electronic states are in quasi equilibrium. The rate of electron transfer (recombination) from a TiO_2 surface electronic state to a hole located on the site associated with that specific state was evaluated as the product of a fixed rate and the Fermi−Dirac probability of occupancy of the electronic state. Such rate was used in the calculation of the waiting time for hole hopping as an additional "competing" charge transfer route during hole diffusion. This effectively introduces different recombination rates for different position of the holes on the surface of the particle. The electronic energies of the electron surface states and the energies of the dye sites used for hole hopping between neighboring dyes were recalculated at the beginning of each experiment.

Simulations of electron−hole recombination shown in Figure 3 were carried out considering a cubic particle as described above where electrons can diffuse in the bulk of the particle and holes can diffuse on the surface of the particle. Given the input values of the electron and hole diffusion coefficients (D_n, D_p), constant charge transfer rates for electrons and holes were calculated using the relations $k_n = 6\,D_n/a^2$ and $k_p = 4\,D_p/a^2$, where a is the lattice spacing. The same value of lattice

DOI: 10.1021/jacs.6b04956
J. Am. Chem. Soc. 2016, 138, 13197−13206

parameter a was used for the bulk (electron diffusion) and the surface of the particle (hole diffusion). Charges could be exchanged between 6 (for electrons) and 4 (for holes) nearest neighbors. The electron and the hole's positions were initially defined randomly within their respective spaces. Recombination times between charges was recorded once the electron and the hole were at a distance equal or lower than $3^{1/2}a$. We ran 10^3 experiments for each condition and we extracted the lifetime ($t_{50\%}$) from the resulting population decay.

■ ASSOCIATED CONTENT

Supporting Information

The Supporting Information is available free of charge on the ACS Publications website at DOI: 10.1021/jacs.6b04956.

TD-DFT calculations and spectroelectrochemical measurement on D131 dye; bias dependent TAS measurements on D131 sensitized TiO_2 films; additional details on experimental and computational method; analysis of dispersion in transient absorption anisotropy decays; simulation of electron hole recombination; dye degradation; MP13 synthesis and properties. (PDF)

■ AUTHOR INFORMATION

Corresponding Authors

*davide.moia11@imperial.ac.uk

*piers.barnes@imperial.ac.uk

Present Address

[‖]Department of Chemistry, Massachusetts Institute of Technology, 77 Massachusetts Avenue, Cambridge, Massachusetts 02139, United States.

Notes

The authors declare no competing financial interest.

■ ACKNOWLEDGMENTS

We thank Xiaoe Li, Shogo Mori and Shane Ardo for useful discussions. DM and PB are grateful for EPSRC fellowship EP/J002305/1. NR thanks EPRSC for grant number EP/H040218/1.

■ REFERENCES

(1) O'Regan, B.; Moser, J.; Anderson, M.; Graetzel, M. *J. Phys. Chem.* **1990**, *94*, 8720.

(2) Tachibana, Y.; Vayssieres, L.; Durrant, J. R. *Nat. Photonics* **2012**, *6*, 511.

(3) Hagfeldt, A.; Boschloo, G.; Sun, L.; Kloo, L.; Pettersson, H. *Chem. Rev.* **2010**, *110*, 6595.

(4) Ardo, S.; Meyer, G. J. *Chem. Soc. Rev.* **2009**, *38*, 115.

(5) Haque, S. A.; Tachibana, Y.; Klug, D. R.; Durrant, J. R. *J. Phys. Chem. B* **1745**, *1998*, 102.

(6) Nelson, J.; Haque, S. A.; Klug, D. R.; Durrant, J. R. *Phys. Rev. B: Condens. Matter Mater. Phys.* **2001**, *63*, 1.

(7) Nelson, J. *Phys. Rev. B: Condens. Matter Mater. Phys.* **1999**, *59*, 374.

(8) Clifford, J. N.; Yahioglu, G.; Milgrom, L. R.; Durrant, J. R. *Chem. Commun.* **2002**, 1260.

(9) Clifford, J. N.; Palomares, E.; Nazeeruddin, M. K.; Grätzel, M.; Nelson, J.; Li, X.; Long, N. J.; Durrant, J. R. *J. Am. Chem. Soc.* **2004**, *126*, 5225.

(10) Johansson, P. G.; Kopecky, A.; Galoppini, E.; Meyer, G. J. *J. Am. Chem. Soc.* **2013**, *135*, 8331.

(11) Bonhôte, P.; Moser, J. E.; Humphry-Baker, R.; Vlachopoulos, N.; Zakeeruddin, S. M.; Walder, L.; Grätzel, M. *J. Am. Chem. Soc.* **1999**, *121*, 1324.

(12) Palomares, E.; Clifford, J. N.; Haque, S. A.; Lutz, T.; Durrant, J. R. *J. Am. Chem. Soc.* **2003**, *125*, 475.

(13) Wenger, B.; Bauer, C.; Nazeeruddin, M. K.; Comte, P.; Zakeeruddin, S. M.; Gratzel, M.; Moser, J.-E. *Proc. SPIE* **2006**, *6325*, 1.

(14) Hasselmann, G. M.; Meyer, G. J. *J. Phys. Chem. B* **1999**, *103*, 7675.

(15) Wang, D.; Mendelsohn, R.; Galoppini, E.; Hoertz, P. G.; Carlisle, R. a; Meyer, G. J. *J. Phys. Chem. B* **2004**, *108*, 16642.

(16) Bonhôte, P.; Gogniat, E.; Tingry, S.; Barbe, C.; Vlachopoulos, N.; Lenzmann, F.; Comte, P.; Grätzel, M. *J. Phys. Chem. B* **1998**, *5647*, 1498.

(17) Hu, K.; Meyer, G. J. *Langmuir* **2015**, *31*, 11164.

(18) Ardo, S.; Meyer, G. J. *J. Am. Chem. Soc.* **2011**, *133*, 15384.

(19) Brennan, B. J.; Durrell, A. C.; Koepf, M.; Crabtree, R. H.; Brudvig, G. W. *Phys. Chem. Chem. Phys.* **2015**, *17*, 12728.

(20) Wang, Q.; Evans, N.; Zakeeruddin, S. M.; Exnar, I.; Grätzel, M. *J. Am. Chem. Soc.* **2007**, *129*, 3163.

(21) Wang, Q.; Zakeeruddin, S. M.; Cremer, J.; Bäuerle, P.; Humphry-Baker, R.; Grätzel, M. *J. Am. Chem. Soc.* **2005**, *127*, 5706.

(22) Moia, D.; Cappel, U. B.; Leijtens, T.; Li, X.; Telford, A. M.; Snaith, H. J.; O'Regan, B. C.; Nelson, J.; Barnes, P. R. F. *J. Phys. Chem. C* **2015**, *33*, 18975.

(23) Moia, D.; Leijtens, T.; Noel, N.; Snaith, H. J.; Nelson, J.; Barnes, P. R. F. *Adv. Mater.* **2015**, *27*, 5889.

(24) Ogawa, J.; Koumura, N.; Hara, K.; Mori, S. *Jpn. J. Appl. Phys.* **2014**, *53*, 1.

(25) O'Regan, B.; Li, X.; Ghaddar, T. *Energy Environ. Sci.* **2012**, *5*, 7203.

(26) Barnes, P. R. F.; Miettunen, K.; Li, X.; Anderson, A. Y.; Bessho, T.; Gratzel, M.; O'Regan, B. C. *Adv. Mater.* **2013**, *25*, 1881.

(27) Yang, W.; Vlachopoulos, N.; Hao, Y.; Hagfeldt, A.; Boschloo, G. *Phys. Chem. Chem. Phys.* **2015**, *17*, 15868.

(28) Moia, D.; Vaissier, V.; López-Duarte, I.; Torres, T.; Nazeeruddin, M. K.; O'Regan, B. C.; Nelson, J.; Barnes, P. R. F. *Chem. Sci.* **2014**, *5*, 281.

(29) Vaissier, V.; Mosconi, E.; Moia, D.; Pastore, M.; Frost, J. M.; De Angelis, F.; Barnes, P. R. F.; Nelson, J. *Chem. Mater.* **2014**, *26*, 4731.

(30) Koster, L. J. a; Mihailetchi, V. D.; Blom, P. W. M. *Appl. Phys. Lett.* **2006**, *88*, 1.

(31) Gottesman, R.; Tirosh, S.; Barad, H.; Zaban, A. *J. Phys. Chem. Lett.* **2013**, *17*, 2822.

(32) Bonhôte, P.; Dias, A.-P.; Armand, M.; Papageorgiou, N.; Kalyanasundaram, K.; Grätzel, M. *Inorg. Chem.* **1996**, *35*, 1168.

(33) Lide, D. R. *CRC Handbook of Chemistry and Physics*; CRC Press: Boca Raton, FL, 2005.

(34) Gould, I. R.; Ege, D.; Moser, J. E.; Farid, S. *J. Am. Chem. Soc.* **1990**, *11*, 4290.

(35) Dang, X.; Hupp, J. T. *J. Am. Chem. Soc.* **1999**, *36*, 8399.

(36) Moser, J. E.; Grätzel, M. *Chem. Phys.* **1993**, *176*, 493.

(37) Yan, S. G.; Prieskorn, J. S.; Kim, Y.; Hupp, J. T. *J. Phys. Chem. B* **2000**, *46*, 10871.

(38) Anderson, A. Y.; Barnes, P. R. F.; Durrant, J. R.; O'Regan, B. C. *J. Phys. Chem. C* **2011**, *115*, 2439.

(39) Vaissier, V.; Barnes, P.; Kirkpatrick, J.; Nelson, J. *Phys. Chem. Chem. Phys.* **2013**, *15*, 4804.

DOI: 10.1021/jacs.6b04956
J. Am. Chem. Soc. 2016, 138, 13197−13206